Supplementary Information (SI) for the manuscript:

Guest-induced magnetic exchange in paramagnetic $[M_2^{II}L_4]^{4+}$ coordination cages

Brechin, Euan (contact); Singh, Mukesh; Etcheverry-Berríos, Alvaro; Vallejo, Julia; Sanz, Sergio; Martínez-Lillo, José; Nichol, Gary; Lusby, Paul

Table of Contents

1. Methods

1.1. Mass Spectrometry

MS of the cage compounds were performed on a Synapt G2 (Waters, Manchester, UK) mass spectrometer using a direct infusion electrospray ionization source (ESI), controlled using Masslynx v4.1 software. All of the scans in the experimental data are for positive ions. Sample **1** was dissolved in acetonitrile at 50 μM. Due to the low solubility of samples **2** − **3**, they were dissolved in acetonitrile with 20 % DMF at 50 μM. Prior to analysis, instruments were calibrated using a solution of sodium iodide (2 mg/mL) in 50:50 water:isopropanol. Capillary voltages were adjusted between 1.5 and 2.5 kV to optimize spray quality, while the sampling cone and the extraction cone voltages were minimised to reduce breakdown of the assemblies. Source temperature was set at 80 °C. The data were analysed using MassLynx v4.1 software.

1.2. *NMR Spectroscopy*

^{1}H and ^{13}C NMR spectra were recorded on a 500 MHz Bruker AV III equipped with a DCH cryo-probe (Ava500). All DOSY experiments were performed using bipolar gradient pulses for diffusion with two spoil gradients (ledbpg2s.compensated) pulse sequence. The sequence was carried out under automated conditions where the duration of the magnetic field pulse gradient (δ) was 1.5 ms and the diffusion time (Δ) was 100 ms. Typically in each PFG NMR experiment, a series of 16 spectra on 32 K data points were collected and the eddy current delay (Te) was set to 5 ms in all experiments. The pulse gradients (g) were incremented from 2 to 95% of the maximum gradient strength in a linear ramp. The temperature was set and controlled at 300 K with an air flow of 400 l h^{-1} in order to avoid any temperature fluctuations due to sample heating during the magnetic field pulse gradients.

1.3. Inductively Coupled Plasma-Optical Emission Spectroscopy

ICP-OES of all compounds were performed on a Perkin Elmer Optima 5300 DV ICP-OES spectrometer. Samples were prepared by dissolution of 3 − 5 mg of sample in 4% aqua regia.

1.4. Magnetic Measurements

Variable-temperature (2.0–270 K) direct current (dc) magnetic susceptibility measurements under an applied field of 0.1 T, and variable field (0–7.0 T) magnetisation measurements at different temperatures (in the range 2.0–7.0 K) were carried out with a Quantum Design SQUID magnetometer.

2. **Synthesis**

All chemicals were of reagent quality, purchased from commercial sources and used without further purification.

2.1 Synthesis of 1,3-bis(3-ethynylpyridyl)benzene (L)

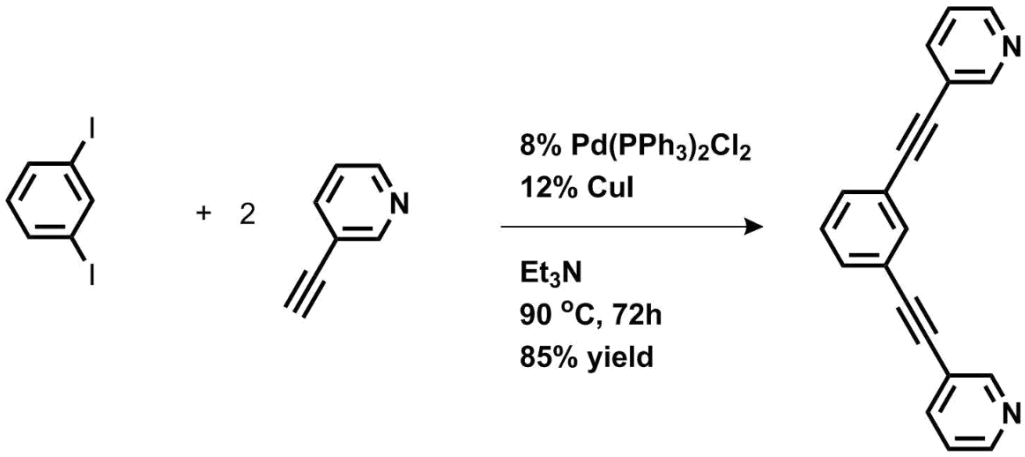

This was made using a procedure slightly modified from the literature.[1] To a 250 mL round-bottomed flask was added 1,3-diiodobenzene (3.9 g, 12 mmol), 3-ethylnylpyridine (2.7 g, 26 mmol), bis-(triphenylphosphine)palladium(II) dichloride (0.67 g, 0.96 mmol) and CuI (0.27 g, 1.4 mmol). The solvent, triethylamine (150 mL), was degassed for 30 minutes before it was added to the reaction mixture. The reaction mixture was refluxed, under N_2, for 72 h. The solvent was evaporated under reduced pressure, dichloromethane (300 mL) was added to the resulting residue. The mixture was filtered and washed with water (3x300 mL) and brine (1x300 mL). Then the organic solvent was further dried using sodium sulfate and the filtered solvent was evaporated under vacuum. The residue was purified by column chromatography on silica gel using CH_2Cl_2 /acetone (9:1) as an eluent. The product was isolated as a light yellow solid, which was further purified by dissolving ~2.8g in 5 mL of CH_2Cl_2 and 45 mL of n-hexane, heating at 70 °C until the final volume was reduced to 30 mL, and filtered hot. The filtered solution was cooled and kept at 2 °C overnight to give 1.8g of the pure, white crystalline product. Yield 54%. ^{1}H NMR (500 MHz, Chloroform-*d*) δ 8.79 (dd, *J* = 2.2, 0.9 Hz, 2H), 8.59 (dd, *J* = 4.9, 1.7 Hz, 2H), 7.83 (dt, *J* = 7.9, 1.9 Hz, 2H), 7.76 (t, *J* = 1.6 Hz, 1H), 7.56 (dd, *J* = 7.8, 1.6 Hz, 2H), 7.40 (t, *J* = 7.8 Hz, 1H), 7.32 (ddd, *J* = 7.8, 4.9, 0.9 Hz, 2H). ^{13}C NMR (126 MHz, Chloroform-*d*) δ 152.42, 148.93, 138.62, 134.86, 131.96, 128.83, 123.22, 123.19, 120.27, 91.69, 86.84. IR: 1414, 1487 ($\nu_{C=C}$) 2223 cm^{-1} ($\nu_C \equiv {}_C$). HRMS (ESI): *m*/*z* calcd for $C_{20}H_{13}N_2^+$ [M+H$^+$] 281.1079; found 281.1099.

*2.2 Synthesis of Cage **1** ($[Cu^{II}_2L_4(H_2O)(OTf)_3](OTf)\cdot MeCN$)*

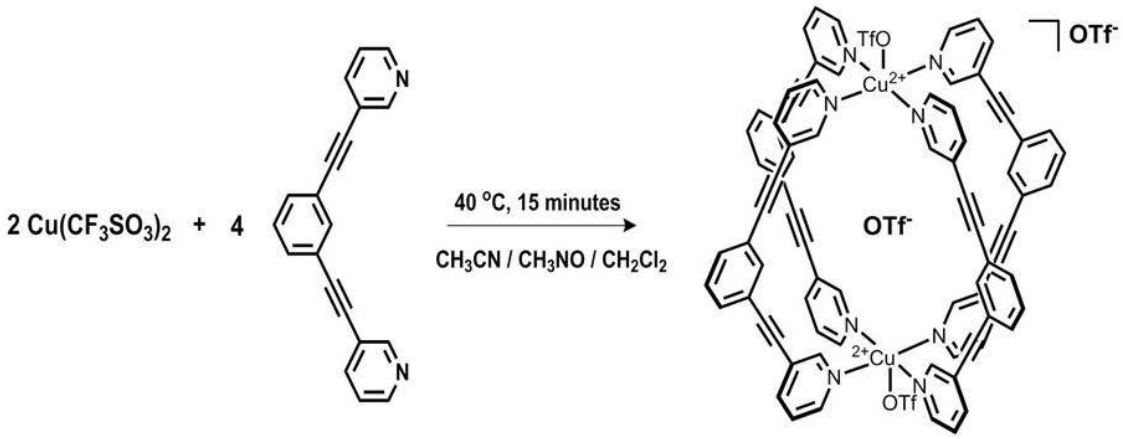

Copper(II) trifluoromethanesulfonate (0.072 g, 0.2 mmol) was dissolved in 4 mL of $MeNO_2$/MeCN (6:1). This solution was added to a CH_2Cl_2 solution (5 mL) of L (0.112 g, 0.4 mmol) under continuous stirring. The deep blue solution was heated at 40 °C for 15 minutes and then filtered. Dark blue X-ray quality crystals were obtained through vapour diffusions of the filtrate with diethyl ether over two days. Yield 85 %. Elemental analysis calculated (%) for $C_{88}H_{56}Cu_2F_{12}N_{10}O_{13}S_4$: C 54.35, H 2.90, N 7.20, S 6.59; found: C 54.23, H 3.01, N 7.21, P 6.57. ICP-OES, calcd 33.75 ppm of Cu and 33.01 ppm of S; found 34.45 and 33.70 ppm of Cu and S, respectively. IR: 1028 ($\nu_{as\ SO3}$), 1056 (ν_{CF3}), 1242 ($\nu_{as\ SO3}$), 1410, 1486 ($\nu_{C=C}$) and 2229 cm^{-1} ($\nu_{C\equiv C}$).

*2.3 Synthesis of Cage **2** ($ReBr_6\subset [Pd^{II}_2L_4](BF_4)_2$)*

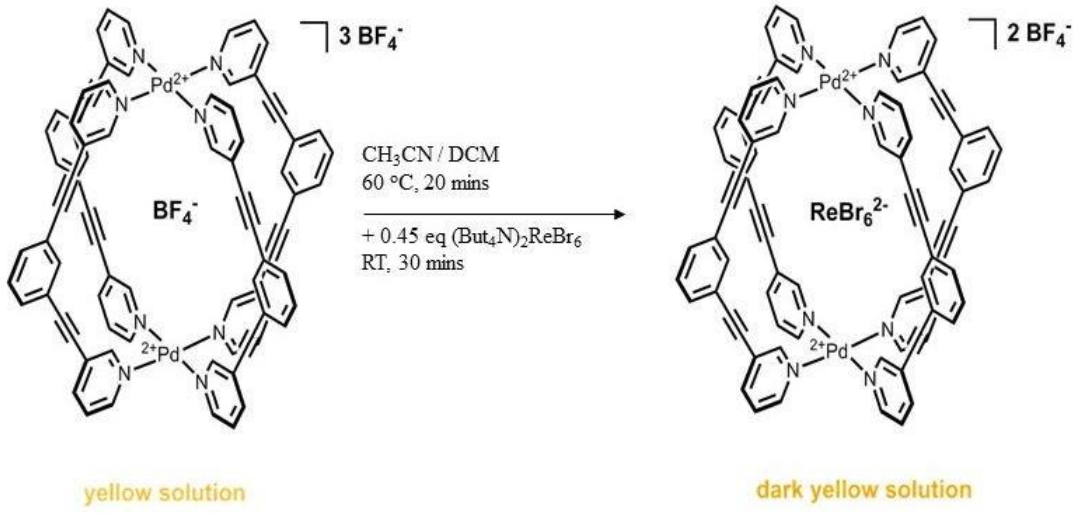

A CH_3CN solution (5 mL) of $[Pd(CH_3CN)_4](BF_4)_2$ (0.0884 g, 0.2 mmol) was added to a CH_2Cl_2 solution (5 mL) of L (0.112 g, 0.4 mmol) under continuous stirring. The yellow solution was heated at 60 °C for 20 minutes. To this solution was added dropwise a CH_2Cl_2 solution (2 mL) of $(Bu^t_4N)_2ReBr_6$ (0.097 g, 0.09 mmol). Dark yellow X-ray quality crystals were obtained through vapour diffusions of the filtrate with pentane over three days. Yield 58 %. Elemental analysis calculated (%) for $C_{86}H_{60}B_2Br_6F_8N_{12}O_4Pd_2Re$: C 43.45, H 2.54, N 7.07, found: C 43.61, H 2.49, N 7.01. ICP-OES calcd 37.71 ppm of Pd, 32.99 ppm of Re and 3.83 ppm of B; found 31.62, 26.63 and 3.21 ppm of Pd, Re and B, respectively. IR: 1053 (ν_{BF4}), 1409, 1480 ($\nu_{C=C}$) and 2223 cm^{-1} ($\nu_{C\equiv C}$).

*2.1 Synthesis of Cage **3** ($ReBr_6\subset [Cu^{II}_2L_4(OTf)_2]$)*

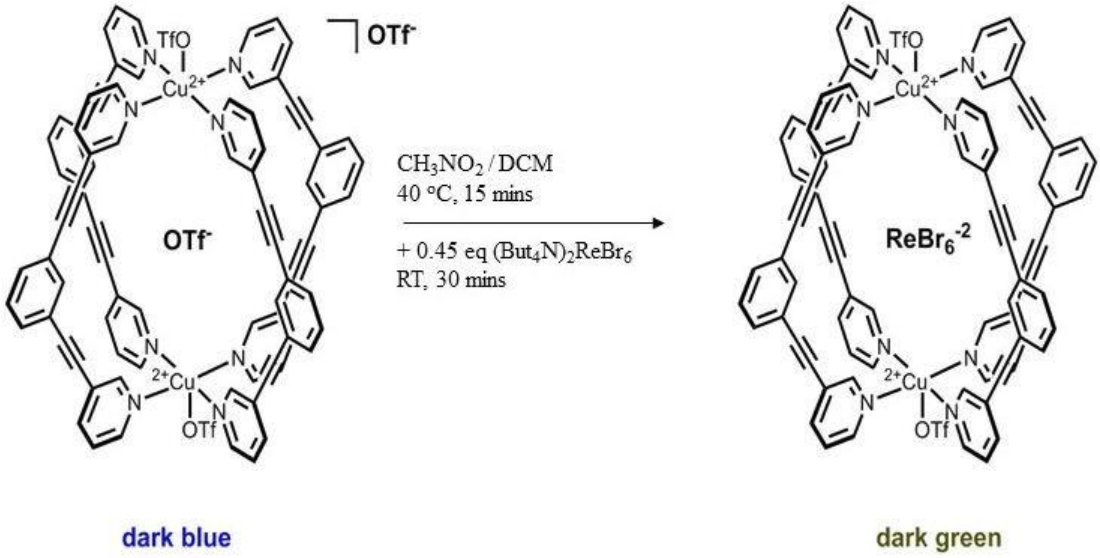

A CH_3NO_2/CH_2Cl_2 solution (4 mL, 6:1) of $Cu(CF_3SO_3)_2$ (0.0722 g, 0.2 mmol) was added to a CH_2Cl_2 solution (5 mL) of L (0.112 g, 0.4 mmol) under continuous stirring. The deep blue solution was heated at 40 °C for 15 minutes and then filtered. A CH_2Cl_2 solution (2 mL) of $(Bu^t_4N)_2ReBr_6$ (0.097 g, 0.09 mmol) was added dropwise to the filtered solution, upon which the colour changed to dark green. Dark green/brown X-ray quality crystals were obtained through vapour diffusions of the filtrate with diethyl ether after one day. Yield 74 %. Elemental analysis calculated (%) for $C_{82}H_{48}Br_6Cu_2F_6N_8O_6ReS_2$: C 44.52, H 2.19, N 5.07, S 2.90; found: C 44.47, H 2.32, N 5.10, S 2.91. ICP-OES calcd 26.51 ppm of Cu, 38.85 ppm of Re and 13.37 ppm of S; found 27.45, 40.43 and 13.89 ppm of Cu, Re and S, respectively. IR: 1029 ($\nu_{s\ SO3}$), 1065 (ν_{CF3}), 1242 ($\nu_{as\ SO3}$), 1408 and 1486 ($\nu_{C=C}$) and 2222 cm^{-1} ($\nu_{C\equiv C}$).

3. Characterization

3.1 Mass Spectrometry

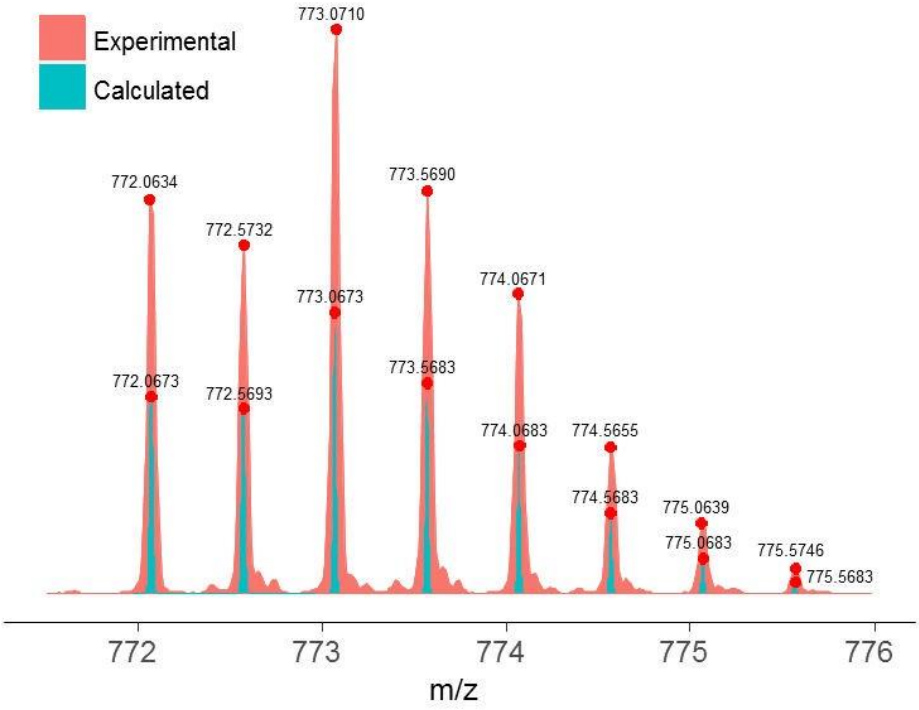

Figure S1. Partial mass spectrum of **1** showing the isotopic distributions of $[Cu_2L_4(OTf)_2]^{2+}$. The experimental data is in red and the simulation in blue.

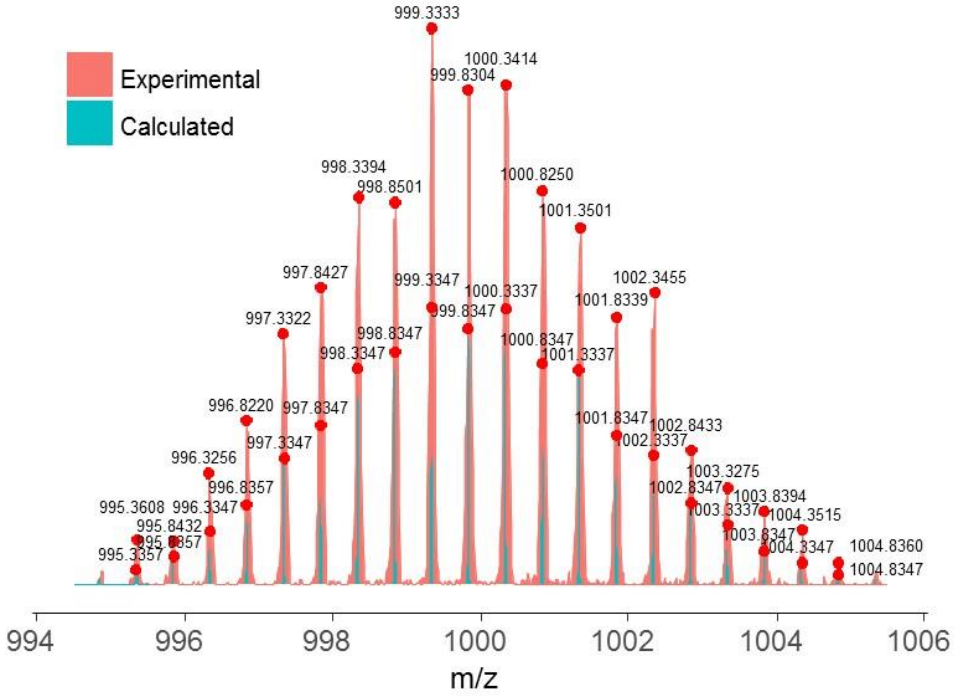

Figure S2. Partial mass spectrum of **2** showing the isotopic distributions of $ReBr_6 \subset [Pd_2L_4]^{2+}$. The experimental data is in red and the simulation in blue.

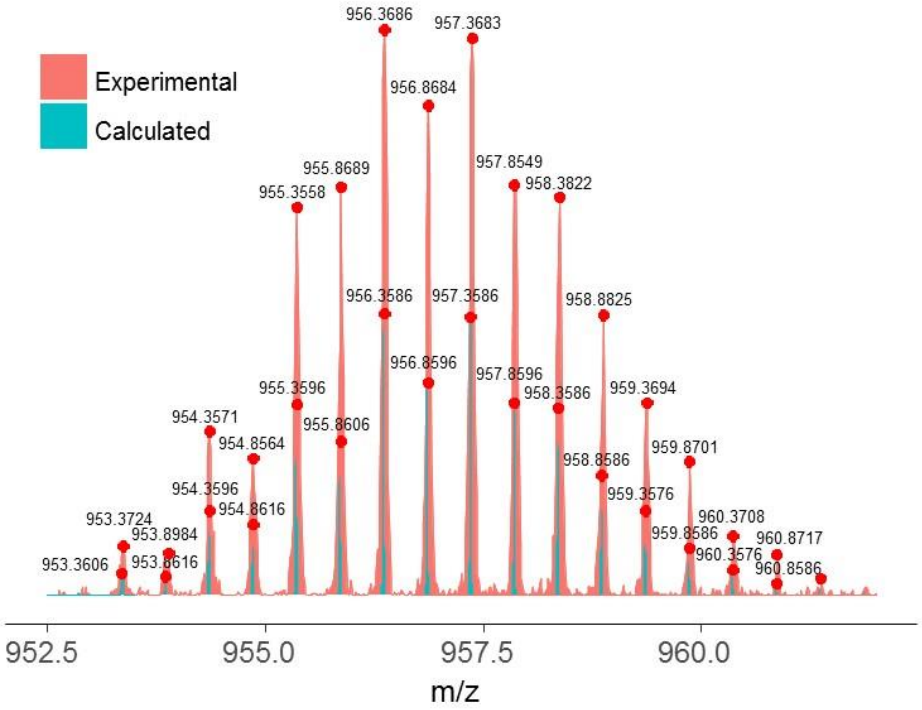

Figure S3. Partial mass spectrum of **3** showing isotopic distributions of $ReBr_6 \subset [Cu_2L_4]^{2+}$. The experimental data is in red and the simulation in blue.

3.2 NMR

3.2.1 NMR of L

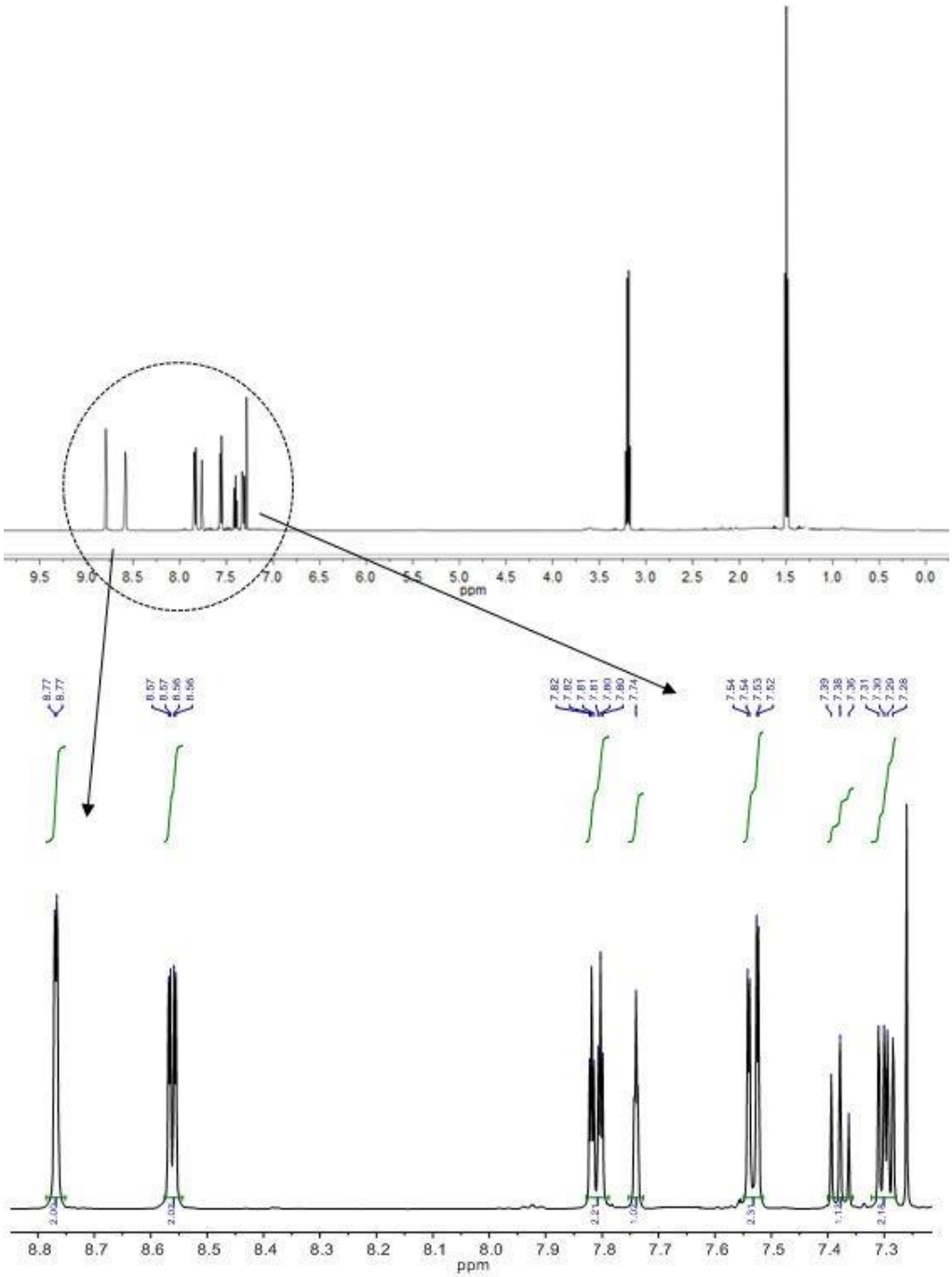

Figure S4. ^{1}H NMR (500 MHz, $CDCl_3$, 300 K) of L.

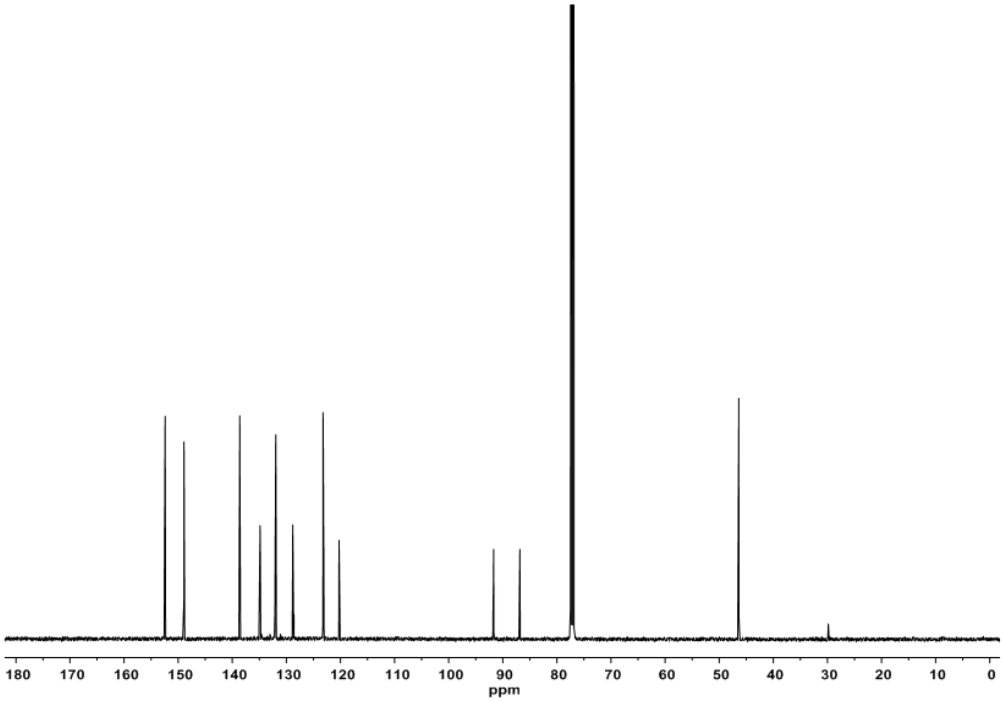

Figure S5. ^{13}C NMR (127.5 MHz, $CDCl_3$, 300 K) of L.

*3.2.2 NMR of **2***

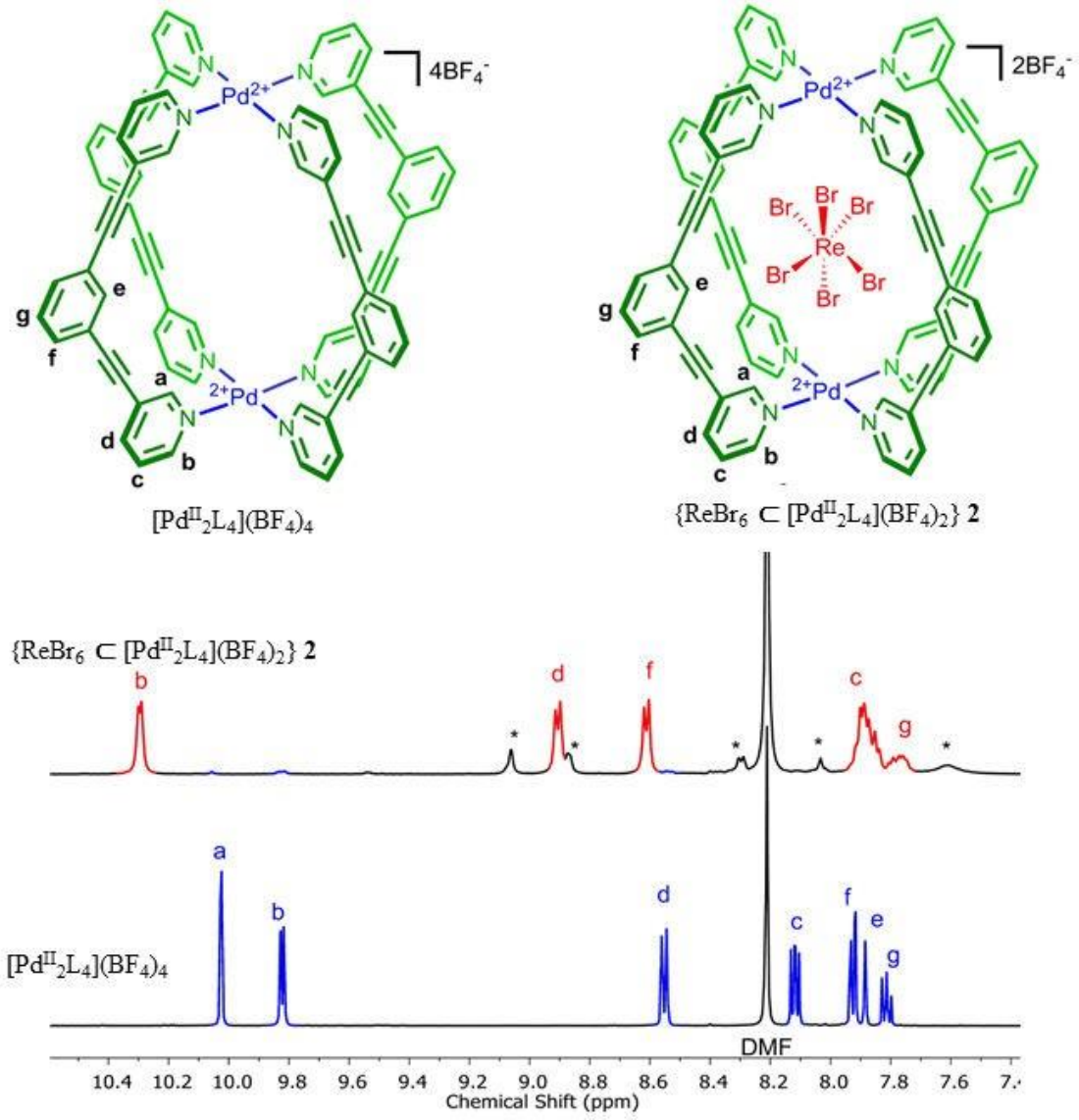

Figure S6. ^{1}H NMR titration spectrum of $[Pd^{II}_{2}L_{4}](BF_{4})_{2}$. One equivalent of $ReBr_{6}^{2-}$ was added as the tetrabutylammonium salt, $(Bu^{t}_{4}N)_{2}ReBr_{6}$. Due to the relatively low solubility of $ReBr_{6}\subset[Pd_{2}L_{4}](BF_{4})_{2}$ (**2**) precipitation was observed during the titration. Free ligand, L, and other L-Pd compounds (marked*) are present at the end of the experiment due to the disassembly of the cage at low concentrations. Experiment performed in DMF-d7 8:2 at 298 K.

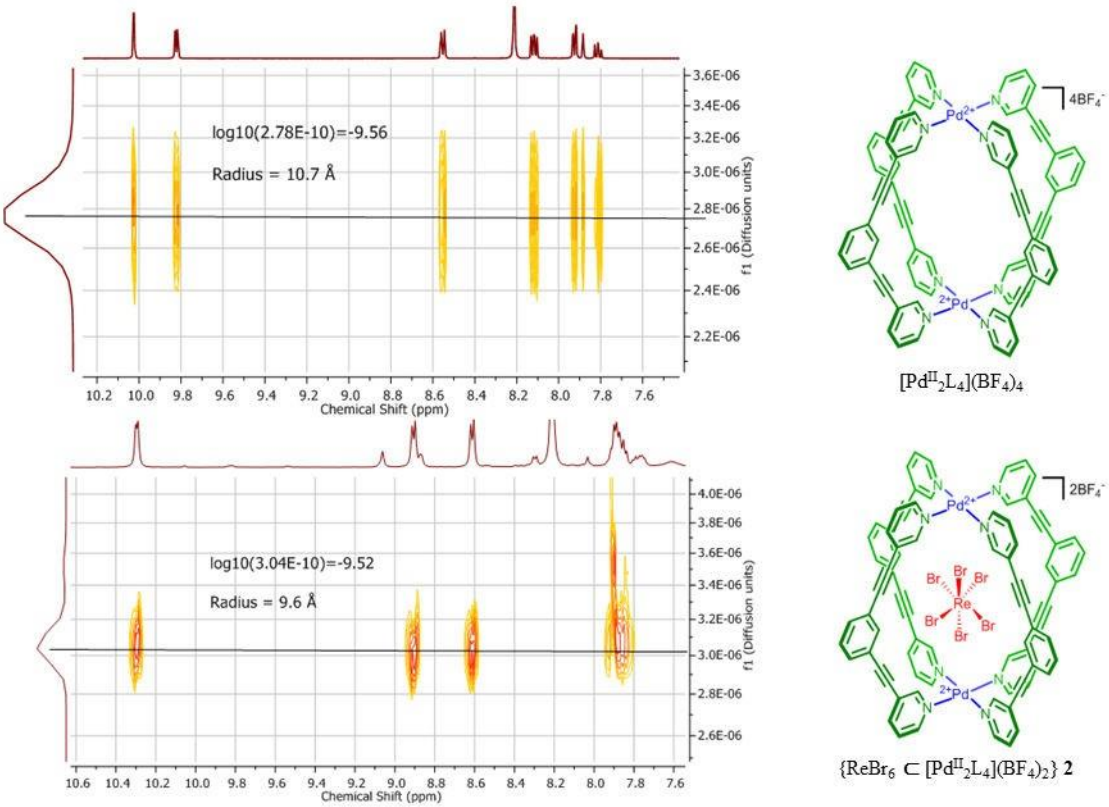

Figure S7. ^{1}H DOSY spectrum of $[Pd^{II}_{2}L_4](BF_4)_2$ (top) and **2** (bottom). Experiment performed in DMF-d7. The hydrodynamic radii determined is ~10 Å, confirming that the guest has been encapsulated in the host cavity.

3.3 X-Ray Structures

Single crystals of **1-3** were selected, coated in Paratone or Fomblin oil and mounted using a MITIGEN mount on either a Bruker SMART APEXII diffractometer (**1**) or a Rigaku Oxford Diffraction SuperNova diffractometer (**2**, **3**) equipped with an Oxford Cryosystems Cryostream 700+ low-temperature device, operating at 120.0 K.

Cell parameters were retrieved using the CrysAlisPro software[2] and refined using CrysAlisPro The structures were solved using Olex2[3] with the ShelXT[4] structure solution program, using the Intrinsic Phasing solution method. The models were refined with version 2014/7 of ShelXL[5] using Least Squares minimisation. All non-hydrogen atoms were refined anisotropically. Hydrogen atom positions were calculated geometrically and refined using the riding model.

Special refinement was carried out for compounds **1-3**. The crystals of **1**, on the microscope slide and at room temperature, appear very well formed. However, when flash cooled at 120 K they give a bad diffraction pattern which was difficult to index. At 200 K the pattern was indexed using CELL_NOW as a non-merohedral twin. The two twin components are related by twin law [-1 0 0 / -0.25 1 -0.73 / 0 0 -1] and refined twin scale factor 0.449(2). One molecule of MeCN was identified but all other electron density pertaining to solvent was handled using the SQUEEZE routine of PLATON. A total of 262 electrons per unit cell were handled this way. It is not really possible to identify the correct solvent ratio from this; 262 electrons roughly correspond with 2.8 molecules of CH_2Cl_2 per asymmetric unit, but the largest residual peak (before using SQUEEZE) was 4.5 electrons high; with CH_2Cl_2 it would be much bigger, even for disordered CH_2Cl_2. The moiety formula is thus reported as "... + solvent". Three of the four triflate anions were modelled as disordered over two sites. Displacement ellipsoid and geometric similarity restraints were used. The data set was cut at a resolution of 1 Å owing to rapidly increasing values of R(merge) at higher resolution.

Compound **2** crystallized as fragile long needles which fractured easily when touched with an acupuncture needle. The crystal could not be cut easily without destroying its integrity so a crystal larger than the X-ray beam was used. Although the cage and counter ions could be identified it was not possible to identify solvent molecules, amounting to some 216 electrons per unit cell. This therefore cannot be included in the total formula, since the identity of the solvent could not be established reliably, and is reported instead as "+ solvent". The SQUEEZE routine of PLATON was used to handle electron density pertaining to the solvent. This triggers checkCIF alerts. The MeCN ligand was refined using an isotropic model. The value of Z' is 0.5. This means that only half of the formula unit is present in the asymmetric unit, with the other half consisting of symmetry equivalent atoms.

For compound **3** a disorder model of the CF_3 group resulted in no better refinement than the ordered model. A region of solvent was modelled as a disordered mix of diethyl ether and nitromethane, consistent with molecular shape inferred from peaks in a difference electron density map. The solvent molecules were refined using an isotropic model and geometric restraints based on average values obtained from a search of the Cambridge Structural Database. While the solvent can be masked using the solvent mask routine in Olex2 to give a cleaner pattern it was felt preferable to report the model which includes the solvent molecules.

The final geometrical calculations and the graphical manipulations were carried out with *PLATON* and *CRYSTALMAKER* programmes.[6] Crystallographic data for the structures reported in this paper have been deposited with the Cambridge Crystallographic Data Centre as supplementary publication no. CCDC–1570738 (**1**), 1570741 (**2**) and 1570740 (**3**). Copies of the data can be obtained free of charge on application to CCDC, 12 Union Road, Cambridge CB21EZ, UK (fax: (+44) 1223-336-033; e-mail: deposit@ccdc.cam.ac.uk).

Table S1. Summary of crystallographic data for **1** – **3**

	1	**2**	**3**
Formula	$C_{86}H_{53}Cu_2F_{12}N_9O_{13}S_4$	$C_{84}H_{54}B_2Br_6F_8N_{10}Pd_2Re$	$C_{88.34}H_{64.69}Br_6Cu_2F_6N_{9.66}O_{10.48}ReS_2$
M (g mol^{-1})	1903.69	2255.45	2400.12
Crystal system	Triclinic	Triclinic	monoclinic
Space group	P-1	P-1	$P2_1/c$
a (Å)	14.0285(6)	12.2191(5)	15.25190(10)
b (Å)	19.1152(9)	12.7370(5)	24.1742(2)
c (Å)	21.1384(11)	20.8002(9)	12.27730(10)
□ (°)	64.740(3)	94.173(3)	90
□ (°)	74.232(3)	105.486(4)	90.7300(10)
□ (°)	78.345(3)	116.145(4)	90
V (Å^3)	4909.3(4)	2731.8(2)	4526.30(6)
Z	2	1	2
Z'	1	0.5	0.5
□$_{calc}$ (g cm^{-3})	1.288	1.371	1.761
μ (mm^{-1})	0.600	7.752	7.278
T (K)	200	120	120
Collcd. reflections	47951	50590	109104
Indep. reflections (R_{int})	13413(0.0869)	11264(0.0734)	9438(0.0659)
Obs. reflections [$I > 2\sigma(I)$]	9503	8451	8666
restraints / parameters	1074 / 1321	0 / 497	21/564
R_1[a] [$I > 2\,\sigma\,(I)$] (all)	0.0991(0.1330)	0.1109(0.1366)	0.0638(0.0686)
wR_2[b] [$I > 2\,\sigma\,(I)$] (all)	0.2639(0.2909)	0.2845(0.3107)	0.1708
Goodness-of-fit	1.028	1.020	1.178

[a] $R_1 = \sum(|F_o| - |F_c|)/\sum|F_o|$. [b] $wR_2 = [\sum w(F_o^2 - F_c^2)^2/\sum w(F_o^2)^2]^{1/2}$.

Table S2. Selected bond distances (Å) and angles (°) for **1**.[a]

	1		**1**
Cu(1)–N(1)	2.055(12)	Cu(2)–N(2)	1.992(11)
Cu(1)–N(3)	2.020(11)	Cu(2)–N(4)	2.032(11)
Cu(1)–N(5)	2.029(12)	Cu(2)–N(6)	2.051(12)
Cu(1)–N(7)	2.029(11)	Cu(2)–N(8)	2.019(11)
Cu(1)–O(1)	2.349(8)	Cu(2)–O(4)	2.321(8)
Cu(1)–O(21)	2.620(9)	Cu(2)–O(7)	2.436(7)
Cu(1)–Br(3)		Cu(1) ⋯Cu(2)	11.532(11)
N(1)–Cu(1)–N(3)	91.0(4)	N(2)–Cu(2)–N(4)	89.8(4)
N(1)–Cu(1)–N(5)	177.1(5)	N(2)–Cu(2)–N(6)	178.3(5)
N(1)–Cu(1)–N(7)	91.4(4)	N(2)–Cu(2)–N(8)	989.6(4)
N(3)–Cu(1)–N(5)	88.6(5)	N(4)–Cu(2)–N(6)	90.8(4)
N(3)–Cu(1)–N(7)	176.3(5)	N(4)–Cu(2)–N(8)	176.0(4)
N(5)–Cu(1)–N(7)	88.9(4)	N(6)–Cu(2)–N(8)	89.7(4)
O(1)–Cu(1)–N(1)	90.4(4)	O(4)–Cu(2)–N(2)	92.9(4)
O(1)–Cu(1)–N(3)	94.8(4)	O(4)–Cu(2)–N(4)	90.1(4)
O(1)–Cu(1)–N(5)	92.5(4)	O(4)–Cu(2)–N(6)	88.7(4)
O(1)–Cu(1)–N(7)	88.0(4)	O(4)–Cu(2)–N(8)	93.9(4)
O(21)–Cu(1)–N(1)	88.6(4)	O(7)–Cu(2)–N(2)	88.2(4)
O(21)–Cu(1)–N(3)	87.3(4)	O(7)–Cu(2)–N(4)	87.8(4)
O(21)–Cu(1)–N(5)	88.5(4)	O(7)–Cu(2)–N(6)	90.2(4)
O(21)–Cu(1)–N(7)	90.0(4)	O(7)–Cu(2)–N(8)	88.2(4)
O(1)–Cu(1)–O(21)	177.7(3)	O(4)–Cu(2)–O(7)	177.6(3)

[a] Estimated standard deviations are given in parentheses.

Table S3. Selected bond distances (Å) and angles (°) for **2.**[a]

	2		**2**
Pd(1)–N(1)	2.036(12)	Pd(1)–N(3)	2.010(12)
Pd(1)–N(2)	2.026(12)	Pd(1)–N(4)	2.007(12)
Pd(1)–Br(2)	4.222(12)		
Pd(1) ⋯Pd(2)	11.827(12)		
N(1)–Pd(1)–N(2)	178.8(6)	N(2)–Pd(1)–N(3)	89.9(4)
N(1)–Pd(1)–N(3)	90.5(4)	N(2)–Pd(1)–N(4)	90.3(5)
N(1)–Pd(1)–N(4)	89.3(5)	N(3)–Pd(1)–N(4)	179.4(6)
Pd(1)–Br(2)–Re(1)	121.26		

[a] Estimated standard deviations are given in parentheses.

Table S4. Selected bond distances (Å) and angles (°) for **3**.[a]

	3		**3**
Cu(1)–N(1)	2.016(6)	Cu(1)–N(3)	2.012(6)
Cu(1)–N(2)	2.015(6)	Cu(1)–N(4)	2.012(6)
Cu(1)–O(1)	2.238(5)		
Cu(1)–Br(3)	4.298(5)		
Cu(1)⋯Cu(2)	12.225(6)		
N(1)–Cu(1)–N(2)	173.9(2)		
N(1)–Cu(1)–N(3)	89.7(2)		
N(1)–Cu(1)–N(4)	88.0(2)		
N(2)–Cu(1)–N(3)	91.2(2)		
N(2)–Cu(1)–N(4)	90.0(2)		
N(3)–Cu(1)–N(4)	168.6(2)		
O(1)–Cu(1)–N(1)	96.0(2)		
O(1)–Cu(1)–N(2)	90.0(2)		
O(1)–Cu(1)–N(3)	92.8(2)		
O(1)–Cu(1)–N(4)	98.5(2)		
Cu(1)–Br(3)–Re(1)	125.85(4)		

[a] Estimated standard deviations are given in parentheses.

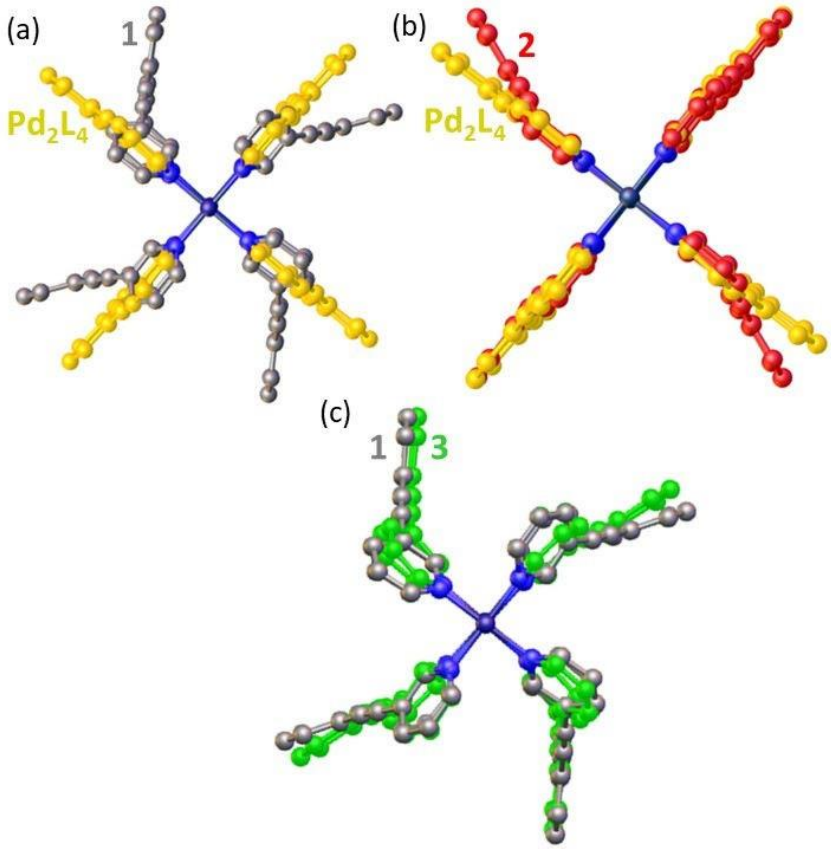

Figure S8. Overlay structures highlighting the changes to the general $[M_2L_4]^{4+}$ framework. (a) $[Pd_2L_4](BF_4)_2$ (yellow) and **1** (grey); (b) $[Pd_2L_4](BF_4)_2$ (yellow) and **2** (red); and (c) **1** (grey) and **3** (green).

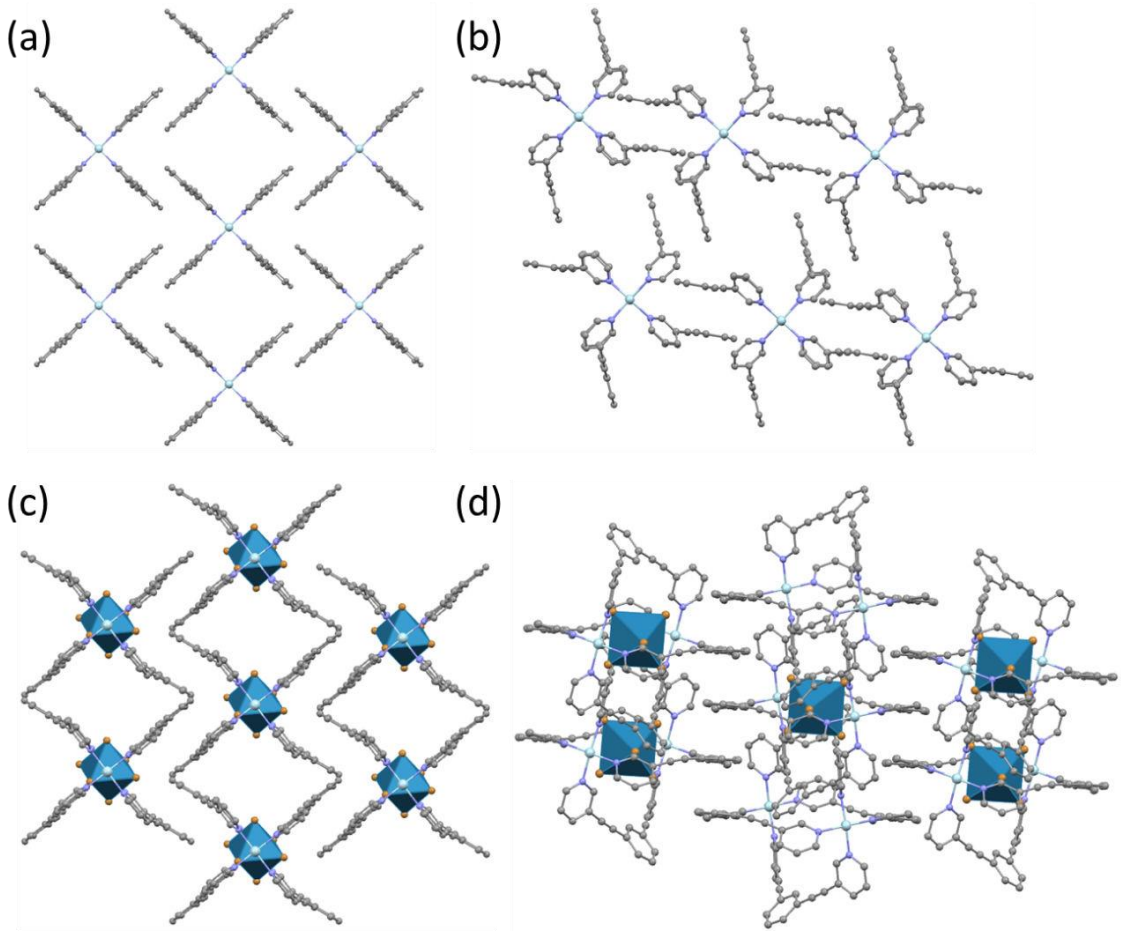

Figure S9. A comparison of partial packing diagrams of (a) $[Pd_2L_4]^{4+}$ (space group *Cm*; CCDC QUPYIK) and **1** (b), **2** (c) and **3** (d) all viewed down the M^{II}-M^{II} axis. All anions and solvent molecules have been removed for clarity. Space groups: **1** = *P*-1, **2** = *P*-1, **3** = $P2_1/c$. In compound **3** there are two different orientations of the cage; in all others there is just one orientation.

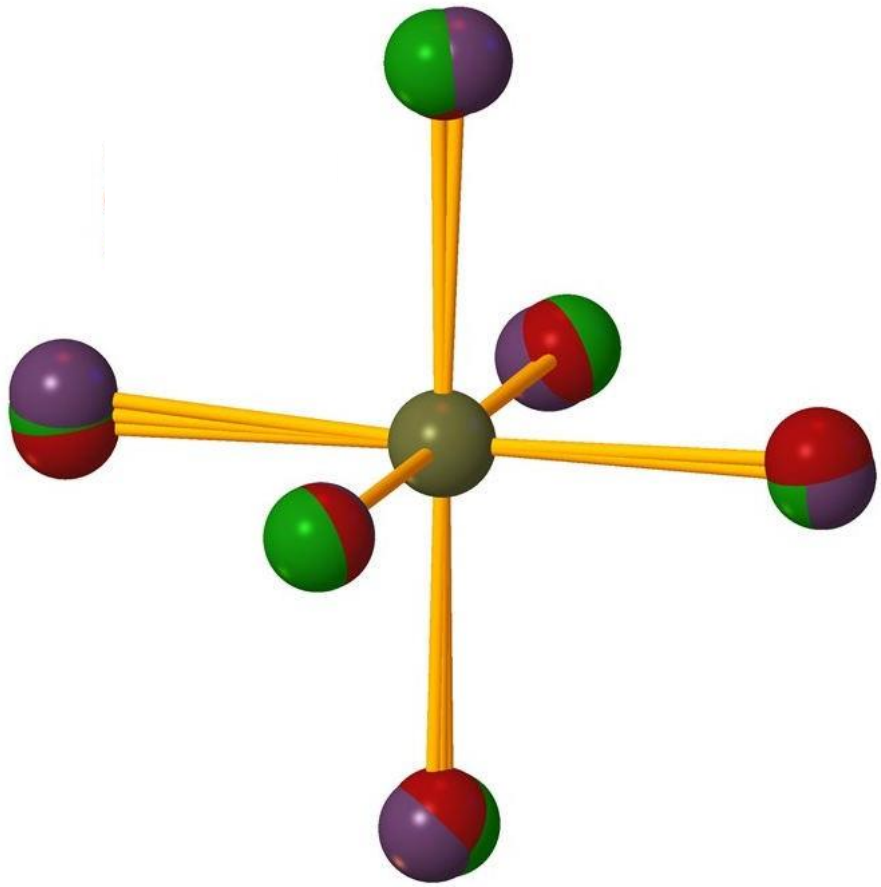

Figure S10. Overlay plot of the $ReBr_6^{2-}$ anion from the salt $(Bu^t_4N)_2[ReBr_6]$ (Br = purple) with the guest $ReBr_6^{2-}$ anions in **2** (Br = red) and **3** (Br = green). The structural similarity would suggest identical, or at least very similar, magneto-anisotropy parameters (D_{Re}) for all three species.

Table S5. SHAPE analysis[8] performed on the $ReBr_6^{2-}$ guests in **2-3**. Small distortions with respect to an ideal octahedral geometry give rise to mixing of excited states, and as a consequence large zero-field splitting is expected. Note that the $ReBr_6^{2-}$ guests in **2-3** possess near-identical distortions and are thus expected to have the same or very similar magneto-anisotropies.

HP-6	**1 D6h**	**Hexagon**
PPY-6	**2 C5v**	**Pentagonal pyramid**
OC-6	**3 Oh**	**Octahedron**
TPR-6	**4 D3h**	**Trigonal prism**
JPPY-6	**5 C5v**	**Johnson pentagonal pyramid J2**

Structure [ML6]	**HP-6**	**PPY-6**	**OC-6**	**TPR-6**	**JPPY-6**
$(ReBr_6)(TBA)_2$	**33.004,**	**28.937,**	**0.047,**	**15.524,**	**32.599**
2	**32.082,**	**29.730,**	**0.028,**	**16.435,**	**33.169**
3	**32.553,**	**30.053,**	**0.025,**	**16.327,**	**33.587**

3.4 Computational Details

To estimate the spin-Hamiltonian parameters for the Re^{IV} and Cu^{II} ions, we have used the ORCA software suite (version ORCA 4.0) on the $ReBr_6^{2-}$ unit of **3** and Model 1 (Figure S12), respectively.[9] In Model 1, we have replaced the Re^{IV} ion with the diamagnetic Hf^{IV} ion. To consider scalar relativistic effects we have used the second-order Douglas-Kroll-Hess (DKH) Hamiltonian. DKH-contracted basis sets were used during the calculation: SARC-DKH-TZVP for Re, Hf and DKH-def2-TZVP for the remaining elements.[10] For Re^{IV}, during state-average complete active space self-consistent field (SA-CASSCF) calculations, five d-orbitals with three electrons (CAS (3electrons/5-4d-orbitals)) were considered in the active space. Ten quartet and forty doublet roots were considered during CASSCF calculations. For Cu^{II}, we have considered five d-orbitals with nine electrons. Five doublet roots were considered during the CASSCF calculation. We have used a special grid of 8 for Re^{IV} and Hf^{IV}; and 6 for the remaining elements. We have also performed N-electron valence state perturbation theory (NEVPT2) to account for the dynamic correlation.[11]

To estimate the magnetic exchange coupling values for **1** and **3**, we have performed density functional theory (DFT) calculations using the Gaussian 16 suite.[12] We have used the hybrid B3LYP-D3 functional[13] together with the TZVP basis set for Cu, Zn;[14] the LANL08(f) basis set for Re;[15] the SDD basis set[16] for Br and the 6-31G** basis set for Cl, S, F, O, N, C and H.[17] We used Noodleman's broken symmetry approach[18] to estimate the magnetic exchange interactions. We have used pairwise exchange interaction calculations by keeping only two paramagnetic centres of interest and replacing the third paramagnetic centre with a diamagnetic ion (Cu^{II} with Zn^{II} and Re^{IV} with Hf^{IV}). This methodology is known to reproduce experimental results reliably for complexes with moderate intra-molecular magnetic exchange interactions.[19] To explain the sign and magnitude of the magnetic exchange interactions, we have performed overlap integral calculations between the singly occupied molecular orbitals of Cu^{II}/Re^{IV} ions.[19] We have also performed natural bonding orbitals (NBOs) analysis to show which interactions facilitate the magnetic interaction.[20] Experimental data were fitted with PHI software.[21]

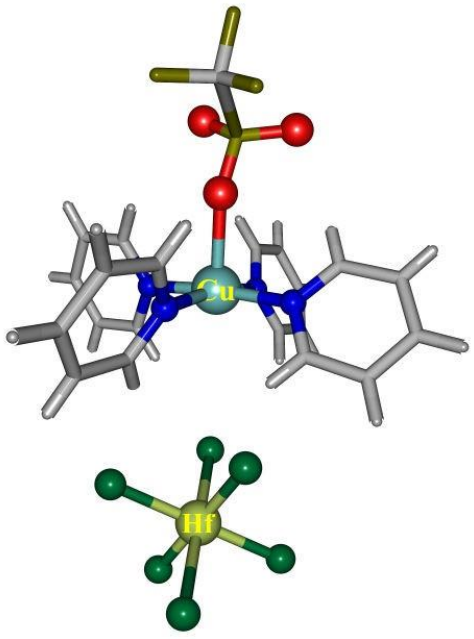

Figure S11. Chemical structure of Model 1, created from **3**, used to estimate the spjn-Hamiltonian parameters in **3**.

Table S6. NEVPT2 calculated individual contributions to D and E/D parameters for the $ReBr_6^{2-}$ guest in **3**. The major contribution to the D parameter is from the spin-flip excitation.

D = +23.0 cm^{-1}, E/D = 0.12 g_{xx}, g_{yy}, g_{zz} (g_{iso}) = 1.747, 1.747, 1.753 (1.749)			
Multiplicity	Root	Contribution to D (cm^{-1})	Contribution to E/D
4	0	0.0	0.0
4	1	31.7	-42.9
4	2	-0.2	19.3
4	3	-28.2	23.6
4	4	0.0	0.0
4	5	0.0	0.0
4	6	0.0	0.0
4	7	0.0	0.0
4	8	0.0	0.0
4	9	0.0	0.0
2	0	0.0	0.0
2	1	0.0	0.0
2	2	0.0	0.0
2	3	0.0	0.0
2	4	0.0	0.0
2	5	232.0	-0.4
2	6	-108.3	109.3
2	7	-103.7	-105.6
2	8	0.0	0.0
2	9	-21.2	26.9
2	10	-1.8	-13.8
2	11	19.9	-13.5
2	12	0.0	0.0
2	13	0.0	0.0
2	14	0.0	0.0
2	15	0.0	0.0
2	16	0.0	0.0
2	17	0.0	0.0
2	18	0.0	0.0
2	19	0.0	0.0
2	20	0.0	0.0
2	21	0.0	0.0
2	22	0.0	0.0
2	23	0.0	0.0
2	24	0.0	0.0
2	25	0.0	0.0
2	26	0.0	0.0
2	27	0.0	0.0
2	28	0.0	0.0
2	29	0.2	-0.1
2	30	0.0	-0.1

2	31	-0.1	0.2
2	32	0.0	0.0
2	33	0.0	0.0
2	34	0.0	0.0
2	35	0.0	0.0
2	36	0.0	0.0
2	37	0.0	0.0
2	38	0.0	0.0
2	39	0.0	0.0

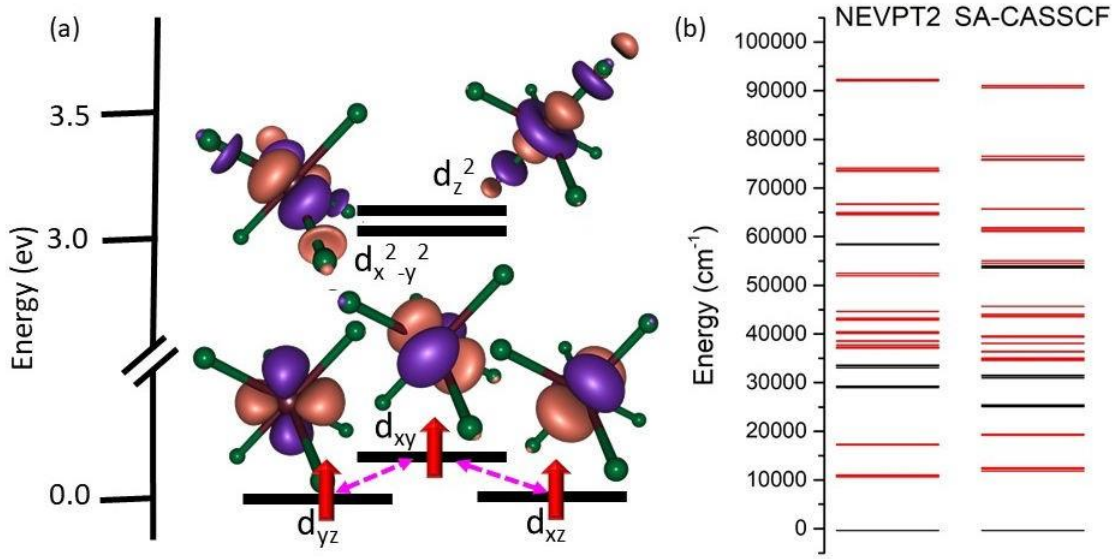

Figure S12. (a) *Ab initio* NEVPT2 and SA-CASSCF computed d-orbital ordering for the $ReBr_6^{2-}$ guest unit of **3** with the iso-density surface plotted with a 0.06 $e^-/bohr^3$ iso-value. The solid red arrows indicate the unpaired electrons and the dotted double headed pink arrows represent the spin-flip electronic transitions which contribute significantly to D_{Re} ($d_{yz/xz} \rightarrow d_{xy}$). Note that the energy difference between the $d_{yz/xz}$ and d_{xy} orbitals is small. This facilitates the spin-flip electronic excitation in $ReBr_6^{2-}$ and thus the large, positive *D* value. (b) *Ab initio* NEVPT2 and SA-CASSCF computed 10 quartet (black) and 40 doublet (red) states for the $ReBr_6^{2-}$ guest unit of **3**. The smaller energy separation between ground quartet and excited doublet states favour spin-flip electronic transitions.

Table S7. DFT computed overlap integrals for **3**. The Re(d_{yz})-Cu(d_{x2-y2}) interaction is found to be the largest contributor to the antiferromagnetic interaction.

	3 {Cu($d_{x^2-y^2}$)}
Re (d_{yz})	0.050
Re (d_{xz})	0.011
Re (d_{xy})	0.013

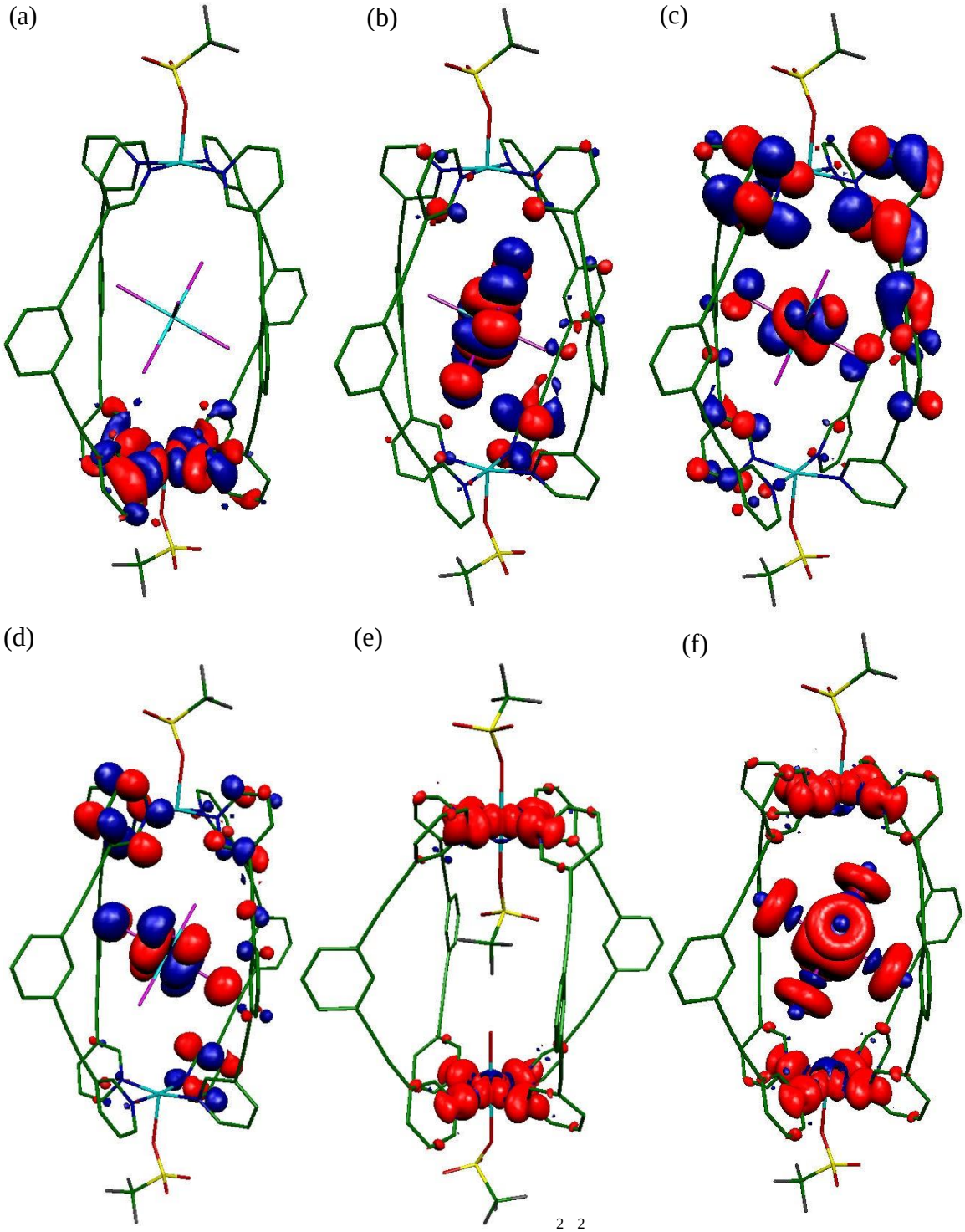

Figure S13. DFT computed spin densities for (a) Cu($d_{x^2-y^2}$); (b) Re(d_{yz}); (c) Re(d_{xz}); (d) Re(d_{xy}); (e) **1** and (f) **3** with the iso-density surface plotted with a 0.02 e^-/bohr^3 iso-value for (a)-(d) and 0.001 e^-/bohr^3 iso-value for (e)-(f).

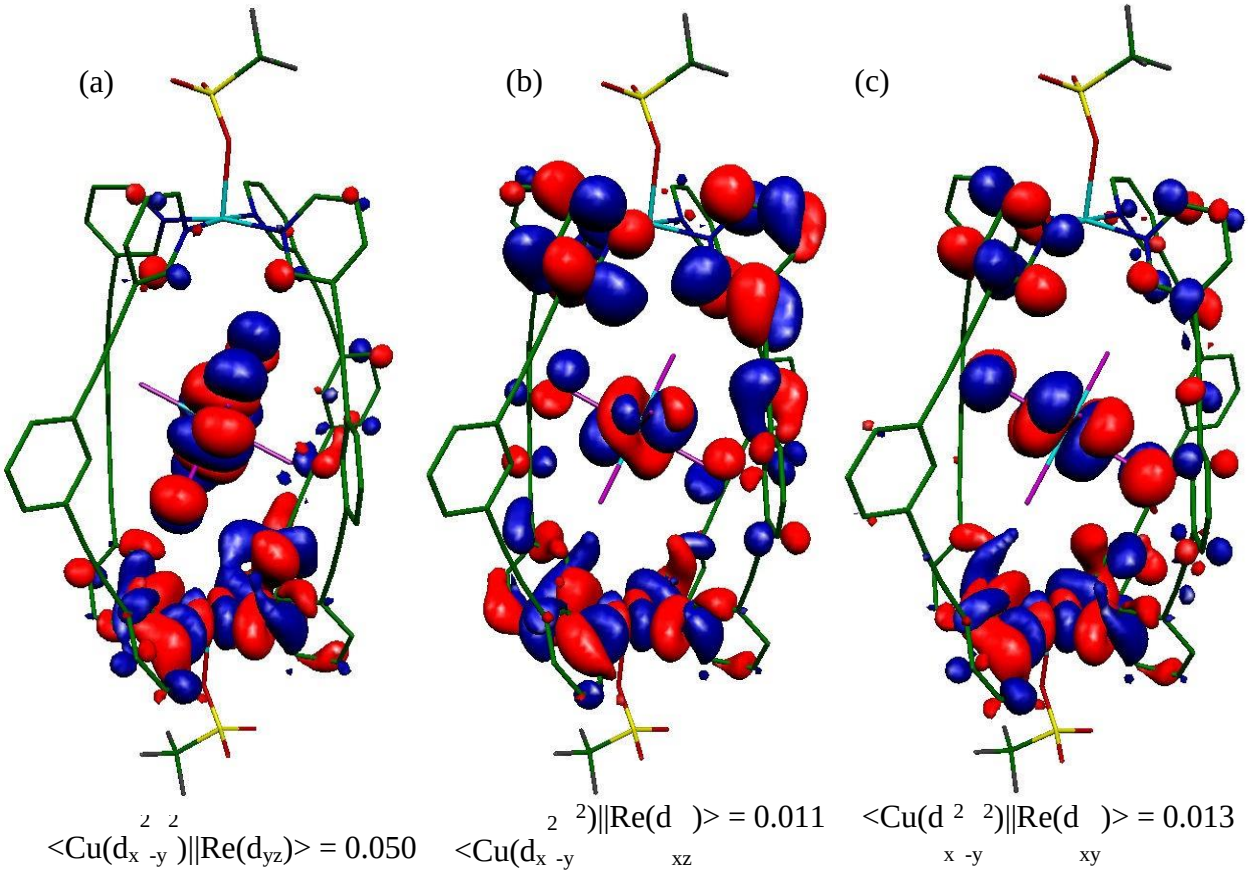

Figure S14. DFT computed overlap integral figures showing the possible SOMO(s)-SOMO(s) interactions in the dimetallic model complex (Zn···Re-Cu) created from **3**. One of the interactions (a; $Cu(d_{x^2-y^2})||Re(d_{yz})$) is found to be the strongest, and is large enough to mediate a significant anti-ferromagnetic interaction. In the other two possible interactions (b-c; $Cu(d_{x^2-y^2})||Re(d_{xz})$ and $Cu(d_{x^2-y^2})||Re(d_{xy})$ respectively), the Re^{IV} magnetic orbitals ($d_{xz/dxy}$) are not directly interacting with the Cu^{II} $d_{x^2-y^2}$ orbital, rather through the long extended π/π^* orbitals of L. The contribution from these two interactions to the magnetic exchange interaction is minimal.

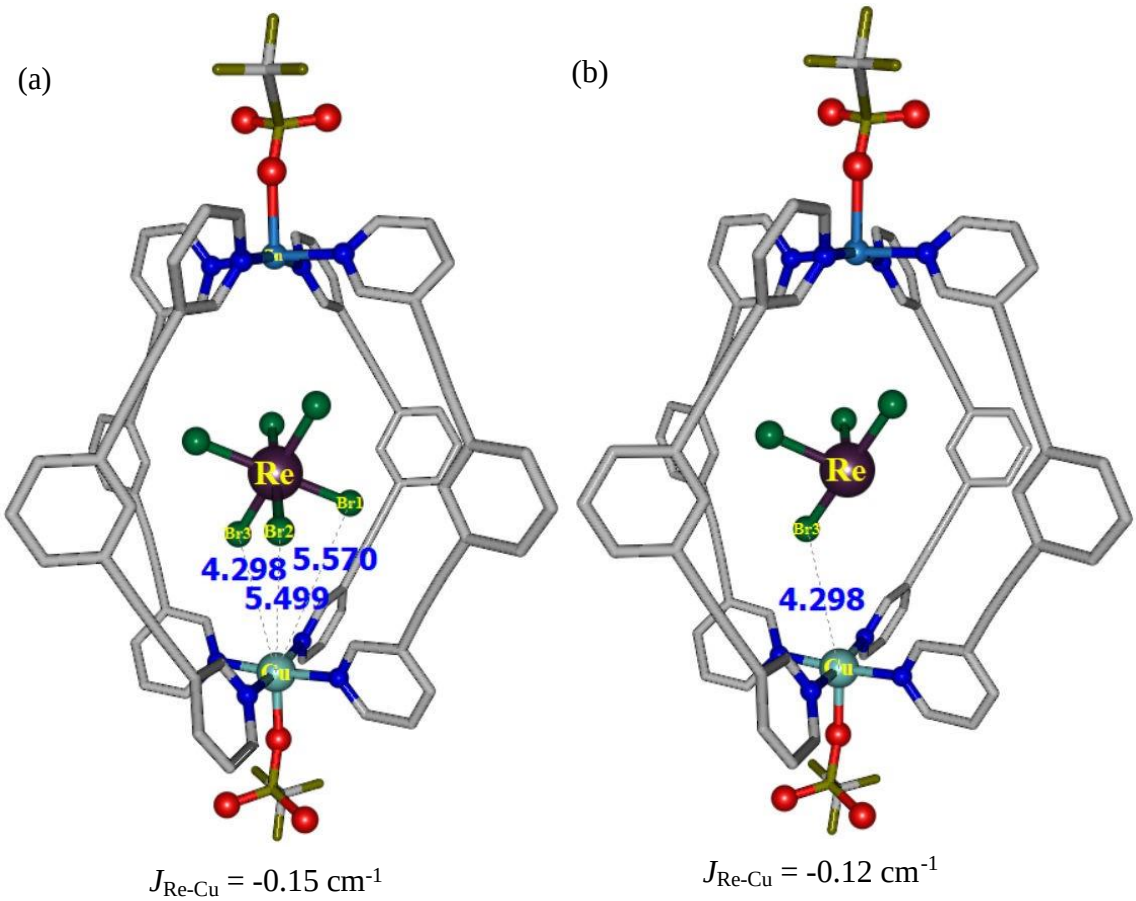

$J_{Re\text{-}Cu}$ = -0.15 cm^{-1} $J_{Re\text{-}Cu}$ = -0.12 cm^{-1}

Figure S15. DFT computed *J* values on model complexes derived from **3**. (a) Dimetallic model complex where one of the Cu^{II} ions is replaced with a Zn^{II} ion. The major contribution to J_{ReCu} is mediated *via* the Re-Br3···Cu pathway. To confirm this, we have constructed another model (b), in which we have replaced Br1 and Br2 with point charges. We observe a minimal decrease in the magnitude of the antiferromagnetic magnetic exchange interaction from -0.15 cm^{-1} to -0.12 cm^{-1}.

Table S8. DFT computed selected NBO orbital interactions (Second Order Perturbation Theory Analysis of Fock Matrix in NBO Basis) between the Br and Cu atoms in **3**.

Interacting hybrid orbitals of Br (Donor)	Interacting Cu orbitals (Acceptor)	Strength of interaction (kcal/mol)
Br3 $\|4s^{0.37}4p_x^{0.63}\|$	Cu $\|4s^{1.0}\|$	0.26
Br3 $\|4s^{0.37}4p_x^{0.63}\|$	Cu $\|4p_x^{1.0}\|$	0.14

4. References

[1] P. Liao, B. W. Langloss, A. M. Johnson, E. R. Knudsen, F. S. Tham, R. R. Julian and R. J. Hooley, *Chem. Commun.*, 2010, **46**, 4932-4934.

[2] CrysAlisPRO Oxford Diffraction /Agilent Technologies UK Ltd, **2015**.

[3] O. V. Dolomanov, L. J. Bourhis, R. J. Gildea, J. A. K. Howard and H. Puschmann, *J. Appl. Crystallogr.*, 2009, **42**, 339–341.

[4] G. M. Sheldrick, *Acta Crystallogr. Sect. A Found. Adv.*, 2015, **71**, 3–8.

[5] G. M. Sheldrick, *Acta Crystallogr. Sect. C Struct. Chem.*, 2015, **71**, 3–8.

[6] (a) A. L. Spek, *Acta Crystallogr. Sect. D, Biol. Crystallogr.*, 2009, **65**, 148; (b) CRYSTALMAKER., D. Palmer, **1996**, Cambridge University Technical Services.

[7] N. R. Voss and M. Gerstein, *Nucleic Acids Res*., 2010, **38**, W555

[8] SHAPE, version 2.0; continuous shape measures calculation; Electronic Structure Group, Universiat de Barcelona: Barcelona, Spain, 2010.

[9] F. Neese, *Wiley Interdiscip. Rev. Comput. Mol. Sci*., 2012, **2**, 73–78.

[10] (a) K. Eichkorn, O. Treutler, H. Öhm, M. Häser and R. Ahlrichs, *Chem. Phys. Lett.* 1995, **242**, 652–660; (b) K. Eichkorn, F. Weigend, O. Treutler and R. Ahlrichs, *Theor Chem Acc.*, 1997, **97**, 119–124.

[11] (a) C. Angeli, R. Cimiraglia, S. Evangelisti, T. Leininger and J.-P. Malrieu, *J. Chem. Phys.*, 2001, **114**, 10252; (b) C. Angeli, R. Cimiraglia and J.-P. Malrieu, *J. Chem. Phys.*, 2002, **117**, 9138; (c) C. Angeli, R. Cimiraglia and J.-P. Malrieu, *Chem. Phys. Lett.*, 2001, **350**, 297–305.

[12] M. J. Frisch, G. W. Trucks, H. B. Schlegel, G. E. Scuseria, M. A. Robb, J. R. Cheeseman, G. Scalmani, V. Barone, G. A. Petersson, H. Nakatsuji, X. Li, M. Caricato, A. V. Marenich, J. Bloino, B. G. Janesko, R. Gomperts, B. Mennucci, H. P. Hratchian, J. V. Ortiz, A. F. Izmaylov, J. L. Sonnenberg, Williams, F. Ding, F. Lipparini, F. Egidi, J. Goings, B. Peng, A. Petrone, T. Henderson, D. Ranasinghe, V. G. Zakrzewski, J. Gao, N. Rega, G. Zheng, W. Liang, M. Hada, M. Ehara, K. Toyota, R. Fukuda, J. Hasegawa, M. Ishida, T. Nakajima, Y. Honda, O. Kitao, H. Nakai, T. Vreven, K. Throssell, J. A. Montgomery Jr., J. E. Peralta, F. Ogliaro, M. J. Bearpark, J. J. Heyd, E. N. Brothers, K. N. Kudin, V. N. Staroverov, T. A. Keith, R. Kobayashi, J. Normand, K. Raghavachari, A. P. Rendell, J. C. Burant, S. S. Iyengar, J. Tomasi, M. Cossi, J. M. Millam, M. Klene, C. Adamo, R. Cammi, J. W. Ochterski, R. L. Martin, K. Morokuma, O. Farkas, J. B. Foresman and D. J. Fox, Wallingford, CT, 2016.

[13] (a) A. D. Becke, *Phys. Rev. A*, 1988, **38**, 3098–3100; (b) A. D. Becke, *J. Chem. Phys.*, 1993, **98**, 5648–5652; (c) C. T. Lee, W. T. Yang and R. G. Parr, *Phys Rev B* 1988, **37**, 785–789.

[14] (a) A. Schäfer, H. Horn and R. Ahlrichs, *J. Chem. Phys.*, 1992, **97**, 2571; (b) A. Schafer, C. Huber and R. Ahlrichs, *J. Chem. Phys.*, 1994, **100**, 5829–5835.

[15] (a) A. W. Ehlers, M. Böhme, S. Dapprich, A. Gobbi, A. Höllwarth, V. Jonas, K. F. Köhler, R. Stegmann, A. Veldkamp and G. Frenking, *Chem. Phys. Lett.*, 1993, **208**, 111-114; (b) P. P. Benjamin, A. Doaa, D. Brett, D. G. Tara and L. W. Theresa, *J. Chem. Inf. Model*.

2019, **59**, 4814-4820.

[16] M. Dolg, U. Wedig, H. Stoll and H. Preuss, *J. Chem. Phys*., 1987, **86**, 866.

[17] V.-A. Rassolov, J.-A. Pople, M.-A. Ratner and T.-L. Windus, *J. Chem. Phys.*, 1998, **109**, 1223–1229.

[18] L. Noodleman, *J. Chem. Phys.*, 1981, **74**, 5737.

[19] (a) M. Coletta, T. G. Tziotzi, M. Gray, G. S. Nichol, M. K. Singh, C. J. Milios and E. K. Brechin, *Chem. Commun.*, 2021, **57**, 4122-4125; (b) D. J. Cutler, M. K. Singh, G. S. Nichol, M. Evangelisti, J. Schnack, L. Cronin, E. K. Brechin, *Chem. Commun.*, 2021, **57**, 8925-8928; (c) M. Coletta, S. Sanz, D. J. Cutler, S. J. Teat, K. J. Gagnon, M. K. Singh, E. K. Brechin and S. J. Dalgarno, *Dalton Trans.*, 2020, **49**, 14790-14797.

[20] (a) J. P. Foster and F. Weinhold, *J. Am. Chem. Soc.*, 1980, **102**, 7211-7218; (b) M. K. Singh, N. Yadav and G. Rajaraman, *Chem. Commun.*, 2015, **51**, 17732.

[21] N. F. Chilton, R. P. Anderson, L. D. Turner, A. Soncini and K. S. Murray, *J. Comput. Chem.*, 2013, **34**, 1164 – 1175.